Article

Polyyn-diyls Capped by Diruthenium Termini: A New Family of Carbon-Rich Organometallic Compounds and Distance-Dependent Electronic Coupling Therein

Guo-Lin Xu, Gang Zou, Yu-Hua Ni, Maria C. DeRosa, Robert J. Crutchley, and Tong Ren

J. Am. Chem. Soc., **2003**, 125 (33), 10057-10065• DOI: 10.1021/ja035434j • Publication Date (Web): 25 July 2003

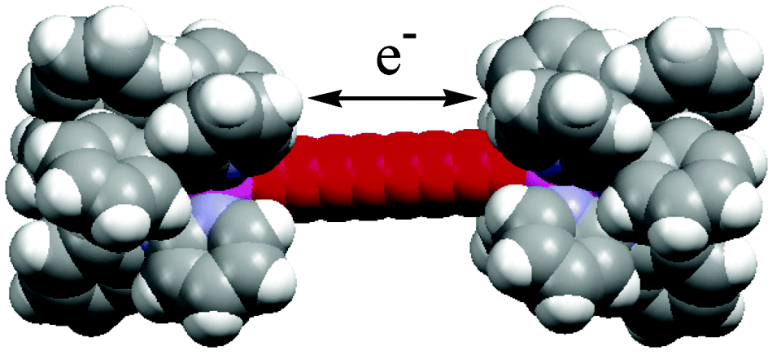

More About This Article

Additional resources and features associated with this article are available within the HTML version:

- Supporting Information
- Links to the 14 articles that cite this article, as of the time of this article download
- Access to high resolution figures
- Links to articles and content related to this article
- Copyright permission to reproduce figures and/or text from this article

View the Full Text HTML

J|A|C|S
ARTICLES
Published on Web 07/25/2003

Polyyn-diyls Capped by Diruthenium Termini: A New Family of Carbon-Rich Organometallic Compounds and Distance-Dependent Electronic Coupling Therein

Guo-Lin Xu,[†] Gang Zou,[†] Yu-Hua Ni,[†] Maria C. DeRosa,[‡] Robert J. Crutchley,*[,‡] and Tong Ren*[,†]

Contribution from the Department of Chemistry, University of Miami, Coral Gables, Florida 33146, and Department of Chemistry, Carleton University, Ottawa, ON K1S 5B6, Canada

Received April 2, 2003; E-mail: tren@miami.edu

Abstract: Polyyn-diyls capped by $Ru_2(ap)_4$ termini (ap = 2-anilinopyridinate), that is, $[Ru_2(ap)_4](\mu\text{-}C,C'\text{-}C_{2m})[Ru_2(ap)_4]$ (compounds **1**−**5** with $m = 1-4$ and 6), were synthesized through either a metathesis reaction between $Ru_2(ap)_4Cl$ and $LiC_{2m}Li$ or a Glaser homocoupling reaction of $Ru_2(ap)_4(C_mH)$ under Eglinton/Hay conditions. X-ray diffraction studies of compounds **2** and **4** revealed both the linear rigid rod topology of these compounds and the fine structural details about the Ru_2 cores and polyyn-diyl chains. Cyclic and differential pulse voltammetric (CV and DPV) measurements and spectroelectrochemical studies show that reduced and oxidized forms of **1**, **2**, **4**, and **5** are donor−acceptor systems in which the Ru_2 termini are coupled to varying degrees depending upon the length of the polyyn-diyl bridge.

The chemistry of metal-alkynyl complexes has attracted long-standing interests from synthetic chemists due to the rich organic transformations that a coordinated alkyne/alkynyl may undergo.[1−4] Attempts to use metallaynes as potential electronic materials can be traced to the studies of rigid rod polymers $[M-(C\equiv C)_m]_n$ with M as Ag, Au, Pd, and Pt in the 1960s.[5,6] Recent developments in carbon-rich materials have brought a renewed interest in using metal-alkynyl complexes as the building blocks for electronic and electrooptic materials, such as molecular electronic devices,[7] nonlinear optical materials,[8] and molecular emitters.[9]

Among various metal-alkynyl complexes synthesized for molecular electronics, polyyn-diyls (C_{2m}) capped by two σ-bonded metal termini, [M], are very attractive prototypes of "organometallic molecular wires" (**I** in Scheme 1).[7,10] Facile electron transport between two [M] termini across the C_{2m} bridge has been elegantly demonstrated with [M] as $CpFe(P-P)$,[11] $CpRe(P)NO$,[12] $CpRu(P)_2$,[13] and $Mn(P-P)_2I$,[14] where P and P−P denote mono- and bidentate phosphines, respectively. For practical applications in molecular electronics, molecules have to meet other criteria in addition to the intrinsic electron/hole mobility: (1) scalability in the range of 10−100 nm and (2) connectivity to the "outside world" (i.e., electrodes and other components of molecular electronic devices).[15] Clearly, monodisperse oligomers consisting of alternating metal and polyyn-diyl units (**II** in Scheme 1) are better alternatives than **I** for achieving length control. In addition, the ability to form oligomer **II** implies the *trans*-ditopic nature of the [M] unit in terms of alkynyl binding, which is also desired for establishing the connectivity to the outside world. However, most of the aforementioned [M] termini are of the Cp-based piano-stool motif and form mono-alkynyl complexes only, which preclude the possibility of the formation of oligomer **II**. Additionally, the judicious selection of the metal center is also critical to achieving wire characteristics.[7] For instance, the insulating behavior of a Pt-metallayne was confirmed through the mechanically controlled break-junction measurement.[16]

Scheme 1. Simple (**I**) and Oligomeric (**II**) Metallayne Wires

[†] University of Miami.
[‡] Carleton University.

(1) *Modern Acetylene Chemistry*; Stang, P. J., Diederich, F., Eds.; VCH: Weinheim, 1995.
(2) Low, P. J.; Bruce, M. I. *Adv. Organomet. Chem.* **2001**, *48*, 71.
(3) Bunz, U. H. F. *Acc. Chem. Res.* **2001**, *34*, 998.
(4) Trost, B. M. *Acc. Chem. Res.* **2002**, *35*, 695.
(5) Nast, R. *Coord. Chem. Rev.* **1982**, *47*, 89.
(6) Hagihara, N.; Sonogashira, K.; Takahashi, S. *Adv. Polym. Sci.* **1980**, *40*, 149.
(7) Paul, F.; Lapinte, C. *Coord. Chem. Rev.* **1998**, *178*−*180*, 431.
(8) Long, N. J. In *Optoelectronic Properties of Inorganic Compounds*; Roundhill, D. M., Fackler, J. P., Eds.; Plenum Press: New York, 1999.
(9) Yam, V. W.-W. *Acc. Chem. Res.* **2002**, *35*, 555.
(10) (a) Bunz, U. H. F. *Angew. Chem., Int. Ed.* **1996**, *35*, 969. (b) Dagani, R. *Chem. Eng. News* **1996**, *Jan. 22*, 22. (c) Lang, H. *Angew. Chem., Int. Ed.* **1994**, *33*, 547. (d) Chisholm, M. H. *Angew. Chem., Int. Ed.* **1991**, *30*, 673.
(11) Le Narvor, N.; Toupet, L.; Lapinte, C. *J. Am. Chem. Soc.* **1995**, *117*, 7129.
(12) (a) Dembinski, R.; Bartik, T.; Bartik, B.; Jaeger, M.; Gladysz, J. A. *J. Am. Chem. Soc.* **2000**, *122*, 810. (b) Brady, M.; Weng, W.; Zou, Y.; Seyler, J. W.; Amoroso, A. J.; Arif, A. M.; Bohme, M.; Frenking, G.; Gladysz, J. A. *J. Am. Chem. Soc.* **1997**, *119*, 775. (c) Zhou, Y.; Seyler, J. W.; Weng, W.; Arif, A. M.; Gladysz, J. A. *J. Am. Chem. Soc.* **1993**, *115*, 8509.
(13) Bruce, M. I.; Low, P. J.; Costuas, K.; Halet, J.-F.; Best, S. P.; Heath, G. A. *J. Am. Chem. Soc.* **2000**, *122*, 1949.
(14) Kheradmandan, S.; Heinze, K.; Schmalle, H. W.; Berke, H. *Angew. Chem., Int. Ed.* **1999**, *38*, 2270.
(15) (a) Tour, J. M. *Acc. Chem. Res.* **2000**, *33*, 791. (b) Ellenbogen, J. C.; Love, J. C. *Proc. IEEE* **2000**, *88*, 386. (c) Carroll, R. L.; Gorman, C. B. *Angew. Chem., Int. Ed.* **2002**, *41*, 4378.

Scheme 2. (4,0)-$Ru_2(ap)_4$ Unit[a]

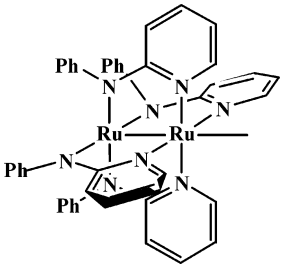

[a] Polyyn-diyl coordinates at the "0" site indicated by the open bond.

Our effort in achieving monodisperse oligomers **II** focuses on using diruthenium paddlewheel species[17] as [M]. Alkynylation chemistry of M−M bonded species began with the synthesis of $Ru_2(ap)_4(C_2Ph)$ in the laboratory of Cotton[18] and was expanded and further explored with M as Mo and W in the laboratory of Hopkins,[19] and M as Rh and Ru in the laboratories of Bear and Kadish,[20] and Ren.[21,22] Notable among many attractive features of the diruthenium building blocks are the controlled syntheses of the mono- and dialkynyl complexes, the stability toward ambient atmosphere and heat, the redox flexibility, and very small HOMO−LUMO gaps (1.2−1.5 eV).[21,22] Previously, we communicated the synthesis of type **I** compounds with [M] as (4,0)-$Ru_2(ap)_4$ (ap = 2-anilinopyridinate, see Scheme 2) and $m = 1$ (**1**) and 2 (**2**) and the electron delocalization between two $Ru_2(ap)_4$ termini therein through cyclic voltammetric (CV) studies.[23] In this contribution, we report the detailed syntheses, structural characterizations, spectroscopic and voltammetric studies of compounds **1**, **2**, and the homologues of longer polyyn-diyl chains, **3**−**5** (m = 3, 4, and 6, respectively), and a spectroelectrochemical investigation of the mixed-valence monoanion and monocation of **2**.

Results

Synthesis. $Ru_2(ap)_4$-capped metallaynes of short polyyn-diyl bridges can be obtained from the metathesis reactions between $Ru_2(ap)_4Cl$ and $LiC_{2m}Li$ (m = 1−3) in satisfactory yields.[23] Because of the thermal instability of longer polyynes, this method becomes less practical with $m \geq 4$. It was found that the Glaser oxidative coupling is a very effective alternative.[24,25] Hence, as shown in Scheme 3, the coupling reaction of $Ru_2(ap)_4(C_2H)$ under Eglinton conditions afforded compound **2**, and reactions of $Ru_2(ap)_4(C_4H)$ and $Ru_2(ap)_4(C_6H)$ under Hay conditions resulted in compounds **4** and **5**, respectively. Most of the $Ru_2(ap)_4$-capped metallaynes have good solubility in THF but not in CH_2Cl_2, which facilitates the removal of impurities through repeated CH_2Cl_2 rinses. Compound **3**, however, is insoluble in all common organic solvents. Compounds **1** and **2** are bluish-purple and reddish-purple, respectively, and **3**−**5** are all dark red. All compounds are indefinitely stable under ambient conditions. The effective magnetic moments per $Ru_2(ap)_4$ range between 3.57 and 4.34 μ_B, indicative of two weakly (or non) interacting $S = {}^3/_2$ centers. The $S = {}^3/_2$ ground state is common among $Ru_2(ap)_4(C_2Y)$ type complexes.[18,21] Although the paramagnetism prevents characterization through NMR spectroscopy, compositions of **1**−**5** were ascertained through both the combustion analysis and the observation of corresponding molecular ions in FAB-MS.

Scheme 3. Synthesis of [Ru_2]-Capped Type I Metallaynes[a]

[a] $Ru_2 = Ru_2(ap)_4$; (i) $LiC_{2m}Li$, THF, m = 1−3; (ii) 3 equiv of $Cu(OAc)_2$, Py; (iii) CuCl/TMEDA, O_2, THF, m = 4, 6.

Crystal and Molecular Structures. Type **I** metallaynes are generally difficult to crystallize, and there are only a limited number of structurally characterized examples containing butadiyn-diyl (C_4)[13,14,26,27] and octotetrayn-diyl (C_8) bridges.[28] Structural examples involving longer C_{12} and C_{16} chains also appeared in the literature recently.[29] X-ray quality crystals for both compounds **2** and **4** were obtained from THF for molecular structure determination. Structural plots of both **2** and **4** are shown in Figure 1, while the selected key metric parameters are collected in Table 1. Clearly, the coordination environment of the Ru_2(II,III) cores in both **2** and **4** resembles those found for $Ru_2(ap)_4(C_2Y)$ type compounds in previous studies.[18,21] The ap ligands adopt the (4,0) arrangement with all anilino N-centers coordinated to one Ru center (4 site) and all pyridine N-centers coordinated to the other Ru center (0 site), which is also σ-bonded to the polyyn-diyl. The Ru−Ru distances in **2** (2.331(2) and 2.333(2) Å) and **4** (2.329(1) Å) are within the range found for other $Ru_2(ap)_4(C_2Y)$ compounds (2.32−2.34 Å). The Ru−C_α distances in **2** and **4** (2.02−2.06 Å) are slightly

(16) Mayor, M.; Hänisch, C. v.; Weber, H. B.; Reichert, J.; Beckmann, D. *Angew. Chem., Int. Ed.* **2002**, *41*, 1183.
(17) Cotton, F. A.; Walton, R. A. *Multiple Bonds between Metal Atoms*; Oxford University Press: Oxford, 1993.
(18) Chakravarty, A. R.; Cotton, F. A. *Inorg. Chim. Acta* **1986**, *113*, 19.
(19) (a) Stoner, T. C.; Dallinger, R. F.; Hopkins, M. D. *J. Am. Chem. Soc.* **1990**, *112*, 5651. (b) Stoner, T. C.; Geib, S. J.; Hopkins, M. D. *J. Am. Chem. Soc.* **1992**, *114*, 4201. (c) Stoner, T. C.; Geib, S. J.; Hopkins, M. D. *Angew. Chem., Int. Ed. Engl.* **1993**, *32*, 409. (d) Stoner, T. C.; Schaefer, W. P.; Marsh, R. E.; Hopkins, M. D. *J. Cluster Sci.* **1994**, *5*, 107. (e) John, K. D.; Geib, S. J.; Hopkins, M. D. *Organometallics* **1996**, *15*, 4357. (f) John, K. D.; Stoner, T. C.; Hopkins, M. D. *Organometallics* **1997**, *16*, 44948. (g) John, K. D.; Miskowski, V. M.; Vance, M. A.; Dallinger, R. F.; Wang, L. C.; Geib, S. J.; Hopkins, M. D. *Inorg. Chem.* **1998**, *37*, 6858.
(20) (a) Yao, C. L.; Park, K. H.; Khokhar, A. R.; Jun, M. J.; Bear, J. L. *Inorg. Chem.* **1990**, *29*, 4033. (b) Li, Y.; Han, B.; Kadish, K. M.; Bear, J. L. *Inorg. Chem.* **1993**, *32*, 4175. (c) Bear, J. L.; Han, B.; Huang, S. *J. Am. Chem. Soc.* **1993**, *115*, 1175. (d) Bear, J. L.; Han, B.; Huang, S.; Kadish, K. M. *Inorg. Chem.* **1996**, *35*, 3012. (e) Bear, J. L.; Li, Y.; Han, B.; Caemelbecke, E. V.; Kadish, K. M. *Inorg. Chem.* **1997**, *36*, 5449. (f) Bear, J. L.; Han, B.; Wu, Z.; Caemelbecke, E. V.; Kadish, K. M. *Inorg. Chem.* **2001**, *40*, 2275.
(21) (a) Ren, T. *Organometallics* **2002**, *21*, 732. (b) Xu, G.; Ren, T. *Organometallics* **2001**, *20*, 2400. (c) Xu, G.; Ren, T. *J. Organomet. Chem.* **2002**, *655*, 239. (d) Hurst, S. K.; Ren, T. *J. Organomet. Chem.* **2002**, *660*, 1. (e) Zou, G.; Alvarez, J. C.; Ren, T. *J. Organomet. Chem.* **2000**, *596*, 152.
(22) (a) Xu, G.; Campana, C.; Ren, T. *Inorg. Chem.* **2002**, *41*, 3521. (b) Lin, C.; Ren, T.; Valente, E. J.; Zubkowski, J. D. *J. Chem. Soc., Dalton Trans.* **1998**, 571. (c) Lin, C.; Ren, T.; Valente, E. J.; Zubkowski, J. D. *J. Organomet. Chem.* **1999**, *579*, 114. (d) Xu, G.; Ren, T. *Inorg. Chem.* **2001**, *40*, 2925.
(23) Ren, T.; Zou, G.; Alvarez, J. C. *Chem. Commun.* **2000**, 1197.
(24) Siemsen, P.; Livingston, R. C.; Diederich, F. *Angew. Chem., Int. Ed.* **2000**, *39*, 2632.
(25) Brandsma, L. *Preparative Acetylenic Chemistry*; Elsevier: Amsterdam, 1988.
(26) Roberts, R. L.; Puschmann, H.; Howard, J. A. K.; Yamamoto, J. H.; Carty, A. J.; Low, P. J. *J. Chem. Soc., Dalton Trans.* **2003**, 1099.
(27) (a) Bruce, M. I.; Hinterding, P.; Tiekink, E. R. T.; Skelton, B. W.; White, A. H. *J. Organomet. Chem.* **1993**, *450*, 209. (b) Akita, M.; Chung, M.-C.; Sakurai, A.; Sugimoto, S.; Terada, M.; Tanaka, M.; Moro-oka, Y. *Organometallics* **1997**, *16*, 4882. (c) Müller, C.; Lachicotte, R. J.; Jones, W. D. *Organometallics* **2002**, *21*, 1190. (d) Gil-Rubio, J.; Laubender, M.; Werner, H. *Organometallics* **1998**, *17*, 1202. (e) Gevert, O.; Wolf, J.; Werner, H. *Organometallics* **1996**, *15*, 2806. (f) Che, C.-M.; Chao, H.-Y.; Miskowski, V. M.; Li, Y.; Cheung, K.-K. *J. Am. Chem. Soc.* **2001**, *123*, 4985. (g) Zhou, Y.; Seyler, J. W.; Weng, W.; Arif, A. M.; Gladysz, J. A. *J. Am. Chem. Soc.* **1993**, *115*, 8509. (h) Yam, V. W. W.; Lau, V. C. Y.; Cheung, K. K. *Organometallics* **1996**, *15*, 1740.
(28) (a) Stahl, J.; Bohling, J. C.; Bauer, E. B.; Peters, T. B.; Mohr, W.; Martín-Alvarez, J. M.; Hampel, F.; Gladysz, J. A. *Angew. Chem., Int. Ed.* **2002**, *41*, 1871. (b) Peters, T. P.; Bohling, J. C.; Arif, A. M.; Gladysz, J. A. *Organometallics* **1999**, *18*, 3261.
(29) (a) Mohr, W.; Stahl, J.; Hampel, F.; Gladysz, J. A. *Inorg. Chem.* **2001**, *40*, 3263. (b) Sakurai, A.; Akita, M.; Moro-oka, Y. *Organometallics* **1999**, *18*, 3241.

Table 1. Selected Bond Lengths (Å) and Angles (deg) for Compounds **2** and **4**

2				**4**	
molecule A		molecule B			
Ru(1)−Ru(2)	2.331(2)	Ru(3)−Ru(4)	2.333(2)	Ru(1)−Ru(2)	2.329(1)
Ru(1)−C(91)	2.05(1)	Ru(4)−C(93)	2.02(2)	Ru(1)−C(1)	2.055(1)
Ru(1)−N(1)	2.08(1)	Ru(3)−N(10)	2.04(1)	Ru(1)−N(1)	2.099(9)
Ru(1)−N(3)	2.08(1)	Ru(3)−N(12)	2.07(1)	Ru(1)−N(3)	2.108(9)
Ru(1)−N(5)	2.08(1)	Ru(3)−N(14)	2.01(1)	Ru(1)−N(5)	2.112(9)
Ru(1)−N(7)	2.09(1)	Ru(3)−N(16)	2.06(1)	Ru(1)−N(7)	2.087(9)
Ru(2)−N(2)	2.07(1)	Ru(4)−N(9)	2.10(1)	Ru(2)−N(2)	2.04(1)
Ru(2)−N(4)	2.04(1)	Ru(4)−N(11)	2.11(1)	Ru(2)−N(4)	2.034(9)
Ru(2)−N(6)	2.05(1)	Ru(4)−N(13)	2.12(1)	Ru(2)−N(6)	2.022(9)
Ru(2)−N(8)	2.06(1)	Ru(4)−N(15)	2.10(1)	Ru(2)−N(8)	2.048(8)
C(91)−C(92)	1.26(2)	C(93)−C(94)	1.24(2)	C(1)−C(2)	1.20(1)
C(92)−C(92A)	1.33(2)	C(94)−C(94A)	1.38(3)	C(2)−C(3)	1.39(2)
				C(3)−C(4)	1.21(2)
				C(4)−C(4A)	1.34(2)
C(91)−Ru(1)−Ru(2)	179.5(4)	C(93)−Ru(4)−Ru(3)	179.8(5)	C(1)−Ru(1)−Ru(2)	177.7(4)
C(92)−C(91)−Ru(1)	178(1)	C(94)−C(93)−Ru(4)	178(2)	C(2)−C(1)−Ru(1)	175(1)
C(91)−C(92)−C(92A)	176(2)	C(93)−C(94)−C(94A)	178(2)	C(1)−C(2)−C(3)	179(2)
				C(4)−C(3)−C(2)	179(2)
				C(3)−C(4)−C(4A)	179(2)

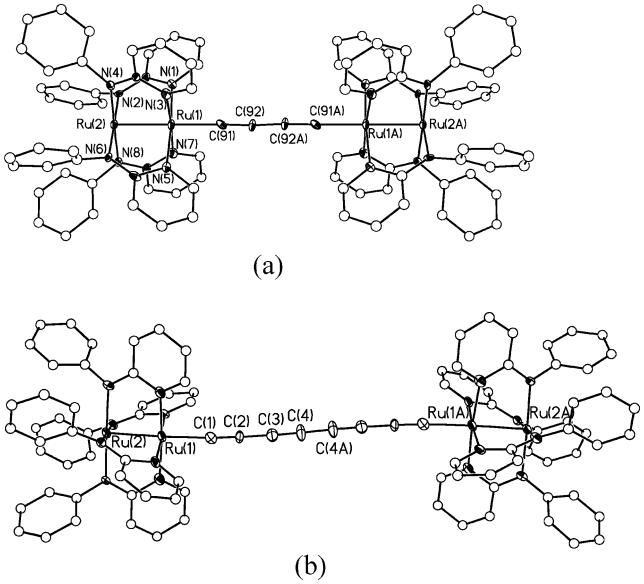

Figure 1. ORTEP plots of molecule **2** (a) and **4** (b) at the 20% probability level. All nonacetylenic carbons are shown as isotropic atoms.

shorter than those found for $Ru_2(ap)_4(C_2Y)$ (2.08−2.10 Å). Shortening of the Ru−C bond indicates that the Ru−C_α interaction is strengthened upon the formation of the type **I** bridged systems.

Carbon−carbon bond length alternation (BLA) in conjugated linear organic systems has attracted tremendous interest from both experimental and theoretical chemists, and the degree of conjugation is generally enhanced as the BLA decreases.[30] Hence, topological features of the polyyn-diyl chain, especially the C≡C and ≡C−C≡ bond lengths, are often the focus of structural studies of type **I** molecules. The BLA of an organic polyyne is much larger than those observed in polyenes and generally agrees with the formalism of alternating triple (1.196−1.203 Å) and single (1.357−1.373 Å) bonds.[31] It is thus

(30) (a) Roncali, J. *Chem. Rev.* **1997**, *97*, 173. (b) van Mullekom, H. A. M.; Vekemans, J.; Havinga, E. E.; Meijer, E. W. *Mater. Sci. Eng., R* **2001**, *32*, 1. (c) Tretiak, S.; Mukamel, S. *Chem. Rev.* **2002**, *102*, 3171.

(31) Toto, J. L.; Toto, T. T.; Melo, C. P. D.; Kirtman, B.; Robins, K. *J. Chem. Phys.* **1996**, *104*, 8586.

Scheme 4. Polyyne and Cumulene Resonance Structures

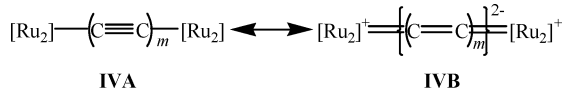

IVA **IVB**

interesting to note that the C≡C bond lengths in **2** (1.26(2) and 1.24(2) Å) were significantly elongated. Elongation of the C≡C bond in **2** is likely attributed to a significant contribution of the cumulenic resonance form (**IVB** in Scheme 4) in addition to the dominating localized polyyne form (**IVA**). Similar C≡C bond elongations were observed in $[I(dppm)_2Mn]_2(\mu\text{-}C_4)$, a molecule that exhibits an extensive electronic delocalization.[14] Nevertheless, one needs to exercise caution not to overinterpret these data because of the inherently low accuracy (large esd) of C−C bond lengths from X-ray diffraction studies. Both the C≡C and the ≡C−C≡ distances and related bond angles determined through X-ray diffraction studies of selected [M]−C_4−[M] compounds were tabulated in a recent publication by Low et al.[26] On the other hand, the C≡C bond lengths (1.20(2) and 1.21(2) Å) in both molecule **4** (Table 1) and other crystallographically characterized [M]−C_8−[M] compounds[28] are much closer to the expected value for the localized C≡C bond.[31]

Scheme 5. Type I Metallaynes of (a) Concave and (b) Sigmoidal Topology

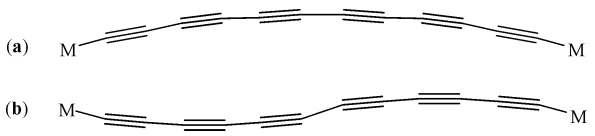

Another noteworthy feature of the polyyn-diyl bridge is the overall curvature of the bridge despite insignificant deviations of the C−C−C bond angles from linearity (less than 5° from 180° in general). The accumulation of the bend generally results in either a subtle sigmoidal or a dramatic concave polyyn-diyl chain (Scheme 5). The former is very common and often involved a crystallographic inversion center that bisects the polycarbon chain. Both molecules **2** and **4** belong in this category. The occurrence of the latter is less frequent, but it has been observed in several Pt-capped type **I** compounds by Gladysz et al.[28,29]

Scheme 6. Assignment of Reversible One-Element Couples

$$[Ru_2^{III,III}\text{---}Ru_2^{III,III}]^{+2} \underset{-e^-}{\overset{+e^-}{\rightleftharpoons}} [Ru_2^{III,III}\text{---}Ru_2^{III,II}]^{+1} \underset{-e^-}{\overset{+e^-}{\rightleftharpoons}} [Ru_2^{III,II}\text{---}Ru_2^{III,II}] \underset{-e^-}{\overset{+e^-}{\rightleftharpoons}} [Ru_2^{II,II}\text{---}Ru_2^{III,II}]^{-1} \underset{-e^-}{\overset{+e^-}{\rightleftharpoons}} [Ru_2^{II,II}\text{---}Ru_2^{II,II}]^{-2}$$

Redox Properties. Type **I** compounds with redox active [M] termini provide an excellent opportunity for the exploration of electron mobility across the polyyn-diyl chains,[7,10] typically via potentiometric studies.[11−14] $Ru_2(ap)_4(C_2SiR_3)$ complexes, the "half" molecules of complexes **1**−**5**, generally exhibit two reversible one-electron processes, a reduction at ca. −0.8 V and an oxidation at ca. 0.45 V.[21] The cyclic voltammograms of compounds **1**, **2**, **4**, and **5** (Figure 2) are clearly more complex than that of $Ru_2(ap)_4(C_2SiR_3)$ and feature multiple one- and two-electron couples. In the case of both **1** and **2**, two one-electron oxidations were observed between 0.2 and 0.50 V, and two one-electron reductions were observed between −0.80 and −1.60 V. The former pair is related to the one-electron oxidation observed for the "half" molecule $Ru_2(ap)_4(C_2SiR_3)$, and the latter is related to the one-electron reduction of $Ru_2(ap)_4(C_2SiR_3)$. The stepwise appearance instead of a two-electron wave is indicative of significant electronic coupling between two $Ru_2(ap)_4$ centers. Several trends are also clear from the comparison of all CV plots and electrode potential data determined from differential pulse voltammetry measurements (DPV, Table 2). (1) As the polyyn-diyl elongates, the difference between $E_{1/2}(+2/+1)$ and $E_{1/2}(+1/0)$ ($\Delta E_{1/2}(+1)$) gradually decreases, indicating that the degree of electronic coupling between two Ru_2 centers decays with the increasing distance. (2) The difference between $E_{1/2}(0/-1)$ and $E_{1/2}(-1/-2)$ ($\Delta E_{1/2}(-1)$) exhibits a similar distance-dependence. (3) For each compound, the $\Delta E_{1/2}(-1)$ value is much larger than the $\Delta E_{1/2}(+1)$ value.

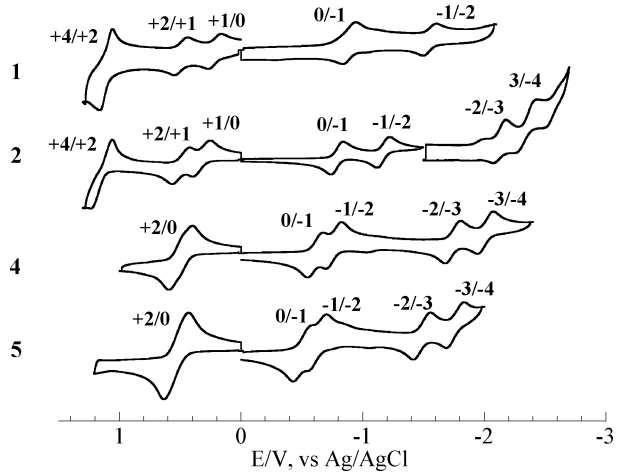

Figure 2. Cyclic voltammograms of compounds **1**, **2**, **4**, and **5** recorded in 0.20 M THF solution of Bu_4NPF_6 at a scan rate of 0.10 V/s.

By comparison with previous studies of the "half molecule" $Ru_2(ap)_4(C_2SiR_3)$, most observed reversible couples can be unambiguously assigned as Ru_2-based as shown in Scheme 6. Also noteworthy is that an additional pair of one-electron reductions, (−2/−3) and (−3/−4), emerged for compound **2** in the very cathodic region. The same pair was readily observed for both **4** and **5**, and potentials for the pair showed a dramatic anodic shift as the polyyn-diyl elongates. In contrast with the pairs already designated as Ru_2-based, the separation between the (−2/−3) and (−3/−4) couples remains about the same for all three compounds and raises the question as to the location of the added electrons. We tentatively assigned these reductions as polyyn-diyl based. On the basis of the particle-in-a-box analogy, one would expect that the elongation of the polyyn-diyl chain stabilizes the lowest π^* orbital and hence results in a significant anodic shift in reduction potentials.

Table 2. Electrochemical Data for Ru_2-Capped Metallaynes from DPV Studies[a]

molecule	+4/+2	+2/+1	+1/0	0/−1	−1/−2	−2/−3	−3/−4
1	1.08	0.47	0.19	−0.87	−1.53	NA	NA
		$K_C(+1) = 54\,000$[b]		$K_C(-1) = 1.4 \times 10^{11}$			
2	1.12	0.47	0.30	−0.81	−1.19	−2.16	−2.39
		$K_C(+1) = 750$		$K_C(-1) = 2.7 \times 10^6$			
4	NA	0.54	0.45	−0.63	−0.78	−1.76	−2.03
		$K_C(+1) = 33$		$K_C(-1) = 343$			
5	NA	0.52 (2e-)		−0.49	−0.62	−1.47	−1.74
		$K_C(+1)$, N/A		$K_C(-1) = 158$			

[a] DPV plots are provided in the Supporting Information. [b] $K_C = \exp(\Delta E_{1/2}/0.0257)$ at 25 °C according to Richardson and Taube.[32]

The potential differences $\Delta E_{1/2}(+1)$ and $\Delta E_{1/2}(-1)$ permit the estimation of comproportionation constants for the corresponding mixed-valence cation ($K_C(+1)$) and anion ($K_C(-1)$), respectively,[32−34] listed in Table 2.

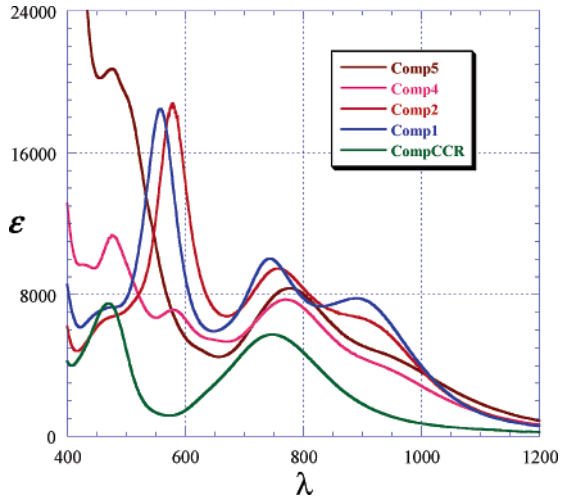

Figure 3. Vis−NIR spectra of compounds **1**, **2**, **4**, and **5** in THF with the extinction coefficients normalized per Ru_2 for comparison to that of $Ru_2(ap)_4(C_2SiMe_3)$ (recorded also in THF, and labeled as CCR).

Electronic Spectroscopy. The vis−NIR spectra of compounds **1**, **2**, **4**, and **5** recorded in THF are shown in Figure 3, along with the spectrum of $Ru_2(ap)_4(C_2SiMe_3)$. Upon the formation of type **I** dimers, the absorption spectra become both intensified and more complicated. For both **1** and **2**, the spectra clearly feature four major transitions: a shoulder at ca. 450 nm, a very intense peak at ca. 570 nm, another intense peak around 750 nm, and a peak (shoulder) around 890 nm. As the polyyn-diyl elongates (**4** and **5**), however, these new features gradually diminish, and the spectra become similar to that of $Ru_2(ap)_4(C_2SiMe_3)$.

(32) Richardson, D. E.; Taube, H. *Inorg. Chem.* **1981**, *20*, 1278.
(33) (a) Crutchley, R. J. *Adv. Inorg. Chem.* **1994**, *41*, 273. (b) Creutz, C. *Prog. Inorg. Chem.* **1983**, *30*, 1.
(34) Launay, J.-P. *Chem. Soc. Rev.* **2001**, *30*, 386.

Scheme 7. Qualitative MO Diagram of $Ru_2(ap)_4(C_2R)$[a]

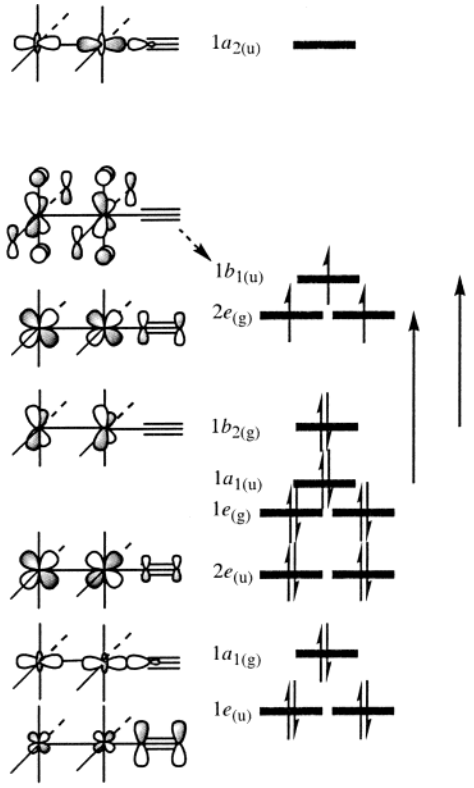

[a] Only the in-plane component of e-type MO is shown; drawings for pure ligand-based MOs $1a_{1u}$ and $1e_g$ were also omitted.

Our analysis began with the assignment of the visible spectrum of the "half" molecule $Ru_2(ap)_4(C{\equiv}CSiMe_3)$, consisting of two intense bands in the visible region (λ_{max}/nm (ϵ, M^{-1} cm^{-1}), in THF): 470 (7500) and 748 nm (5740).[21] A qualitative MO diagram for $Ru_2(HNC(H)NH)_4(CCH)$ shown in Scheme 7 was constructed by combining the result from an Xα calculation of the $Ru_2(HNC(H)NH)_4$ model molecule[35] and orbital contributions from $-C{\equiv}C-$ fragment, where the parity from the $Ru_2(HNC(H)NH)_4$ calculation is retained and parenthesized in the subscript. Clearly, the MOs of significant Ru−Ru characters are, in the ascending order of orbital energy, σ ($1a_{1g}$), π ($2e_u$), δ ($1b_{2g}$), π^* and δ^* ($2e_g$ and $1b_{1u}$, HOMOs), and σ^*($1a_{2u}$, LUMO). Both π^* and δ^* are half-filled, which is in agreement with the observed $S = {}^3/_2$ ground state for $Ru_2(ap)_4(C_2Y)$. On the basis of this scheme, the lowest dipole-allowed transition is clearly the $\delta \rightarrow \delta^*$ transition (low energy), which contains a partial MLCT character because of a significant contribution of N-based π-type orbitals to the δ^* orbital and hence exhibits the high extinction coefficient.

Less certain is the assignment of the high-energy transition observed at 470 nm, which was designated as π(Ru−Cl, Ru_2) $\rightarrow \pi^*(Ru_2)/\delta^*(Ru_2)$ in the case of $Ru_2(ap)_4Cl$.[36] An analogous assignment in the case of $Ru_2(ap)_4(C{\equiv}CSiMe_3)$ would be π(Ru−C, Ru_2) $\rightarrow \pi^*(Ru_2)/\delta^*(Ru_2)$. From Scheme 7, this assignment is unlikely due to the fact that the Xα calculation of $Ru_2(HNC(H)NH)_4$ placed the $\pi(Ru_2)$ orbital ($2e_u$) significantly below the HOMO. Upon the inclusion of C_2SiMe_3, the $\pi(Ru_2)$ orbital becomes slightly destabilized by the filled−filled

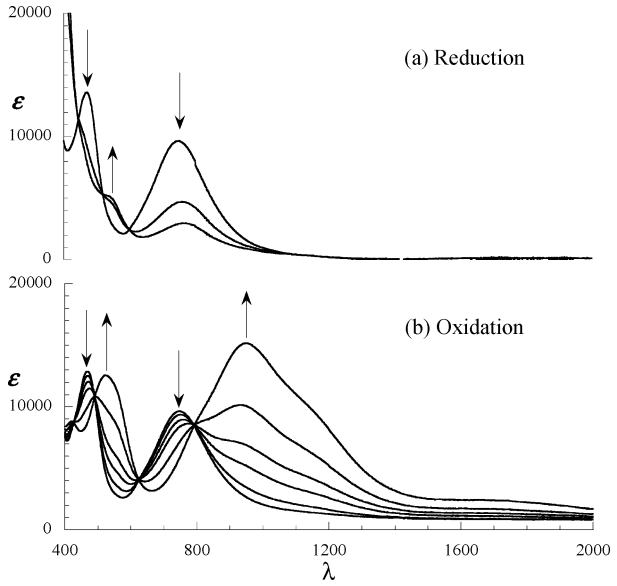

Figure 4. Spectroelectrochemistry of $Ru_2(ap)_4(C_2SiMe_3)$ in THF.

interaction with $\pi(C{\equiv}C)$ ($1e_u$) in $Ru_2(ap)_4(C{\equiv}CSiMe_3)$.[37] While the $\pi(Ru_2) \rightarrow \pi^*(Ru_2)$ transition would be dipole allowed, the energy of the transition would be too high to be observed in the visible region. On the other hand, two π(N) orbitals ($1e_g$ and $1a_{1u}$) are placed immediately below the $\delta(Ru_2)$ orbital in the Xα result,[35] and this arrangement should be unaltered in $Ru_2(ap)_4(C{\equiv}CSiMe_3)$ because both orbitals have minimum, if any, interactions with the axial $C{\equiv}CSiMe_3$ group. The $1a_{1u} \rightarrow 2e_g$ transition is the only dipole-allowed $\pi(N) \rightarrow \pi^*/\delta^*(Ru_2)$ transition, and hence it is assigned to the intense absorption observed at 470 nm. Because of the significant contribution of $\pi^*(C{\equiv}C)$ in $2e_g$, the transition at 470 nm should be sensitive to the nature of the axial ligand. Indeed, there is a 50% increase in intensity from $Ru_2(ap)_4Cl$ to $Ru_2(ap)_4(C{\equiv}CSiMe_3)$.

The assignment of these bands to LMCT transitions is further supported by spectroelectrochemical studies. Figure 4 shows the spectral changes associated with the one-electron reduction (Figure 4a) and oxidation (Figure 4b) of $Ru_2(ap)_4(C_2SiMe_3)$ in THF. The spectroelectrochemical oxidation and reduction of $Ru_2(ap)_4(C_4SiMe_3)$ is very similar to that of $Ru_2(ap)_4(C_2SiMe_3)$ and has been placed in the Supporting Information. In Figure 4a, reduction results in the rapid loss of intensity for both transitions and the appearance of a new band at 580 nm. Appearance of the new band is largely due to a drastic change in the ground-state configuration from $(\pi^*\delta^*)^3$ for Ru_2(II,III) to π^{*4} for Ru_2(II,II).[35] Figure 4b shows the oxidation of the complex in which both bands are red-shifted as the result of the stabilization of Ru_2 d-orbitals. While the intensity of the high-energy band is retained, the intensity of the low-energy band has dramatically increased. The oscillator strength of charge-transfer transitions is proportional to metal−ligand coupling[38] and reflected in the increased contribution of the π(N) characters to the δ^* orbital in the oxidized $Ru_2(ap)_4(C_2SiMe_3)$.

With the spectral assignment of $Ru_2(ap)_4(C_2SiMe_3)$ in hand, we offer a plausible explanation for the rich spectral features

(35) Cotton, F. A.; Ren, T. *Inorg. Chem.* **1991**, *30*, 3675.
(36) Miskowski, V. M.; Hopkins, M. D.; Winkler, J. R.; Gray, H. B. In *Inorganic Electronic Structure and Spectroscopy*; Solomon, E. I., Lever, A. B. P., Eds.; Wiley: New York, 1999; Vol. 2, pp 343−402.
(37) (a) Lichtenberger, D. L.; Renshaw, S. K.; Bullock, R. M. *J. Am. Chem. Soc.* **1993**, *115*, 3276. (b) Lichtenberger, D. L.; Renshaw, S. K.; Wong, A.; Tagge, C. D. *Organometallics* **1993**, *12*, 3522.
(38) Creutz, C.; Newton, M. D.; Sutin, N. *J. Photochem. Photobiol., A* **1994**, *82*, 47.

Scheme 8. Chromophore Orbitals of Dimer Derived from Ru_2-Terminus

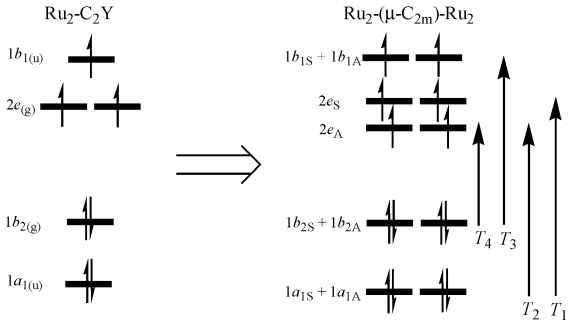

observed for compounds **1**−**5**. With these compounds being considered as the "dimers" of $Ru_2(ap)_4(C_2SiMe_3)$, the MOs responsible for the observed transitions are derived from the combination of those from two equivalent halves. Each MO ψ in $Ru_2(ap)_4(C_2SiMe_3)$ results in a pair of MOs with one symmetric (subscript S) and the other antisymmetric (subscript A) with regard to the inversion center, as shown in Scheme 8. For combinations derived from $1a_{1u}$, $1b_{2g}$, and $1b_{1u}$, the absence of orbital contribution from the C≡C fragment dictates that the symmetric and antisymmetric components remain degenerate. On the other hand, the $2e_g$ orbital contains a substantial contribution from π^*(C≡C) and leads to a small but significant energy splitting between the symmetric ($2e_S$) and antisymmetric ($2e_A$) components. Consequently, two dipole-allowed, but energetically differentiated $\pi(N) \rightarrow \pi^*(Ru_2)$ transitions are observed, as indicated by arrows T_1 and T_2 in Scheme 8. Retention of the degeneracy for both δ and δ^* orbitals implies a single $\delta \rightarrow \delta^*$ transition (T_3), which is observed in all "dimers" as a single peak around 750 nm. In addition, while the $\delta \rightarrow \pi^*$ transition is forbidden in $Ru_2(ap)_4(C_2SiMe_3)$ because of both δ and π^* being gerade, a transition from $1b_{2S} \rightarrow 2e_A$ (T_4) is weakly allowed and appears as the peak (shoulder) observed at ca. 890 nm for both **1** and **2**. Hence, the novel features that distinguished the "dimers" from the "half" molecules are largely due to the orbital mixing through π^* (polyyn-diyl) orbitals. Naturally, the degree of mixing is reduced greatly with the elongation of the polyyn-diyl chain, and dimers of longer chains bear strong spectral resemblance to that of $Ru_2(ap)_4(C_2SiMe_3)$.

Spectroelectrochemistry of Mixed-Valence Complexes. Large K_C values calculated for both the monocations and the monoanions of compounds **1** and **2** imply significant stabilities of these mixed-valence species, and hence it should be possible to observe the intervalence transitions between donor and acceptor Ru_2 moieties as being mediated by the polyyn-diyl bridge.[33,34,39] Compound **2** was selected over **1** for a detailed spectroelectrochemical study because of its better solubility in THF. Unfortunately, the two-electron reduction product of **2** was unstable, which prevented further spectroscopic probing of highly reduced species.

Figure 5a shows electronic absorption spectra of the reversible one-electron reduction product of **2** in THF. Upon reduction, the intense bands at 17 300 and 13 210 cm^{-1} decrease in intensity, and a very broad new band appears at ca. 20 000 cm^{-1}. In addition, the growth of two new bands was observed at 8430 and 5600 cm^{-1}. These low-energy bands are not a characteristic of the reduction of $Ru_2(ap)_4(C_2SiMe_3)$ (Figure 4a) and are

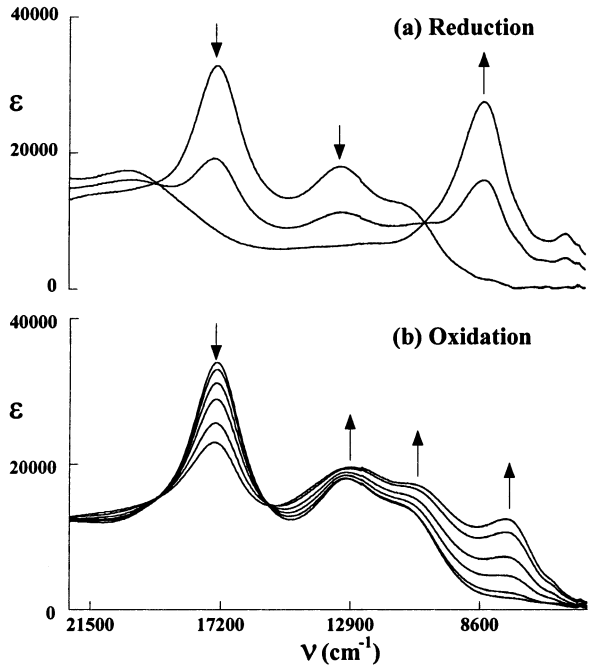

Figure 5. Spectroelectrochemistry of **2** recorded in THF.

therefore assigned to intervalence charge-transfer transitions (IVCT). Deconvolution of the bands assuming a Gaussian band shape yielded the following spectroscopic data: for E_{IVCT} = 8450 cm^{-1}, ϵ = 27 000 M^{-1} cm^{-1}, $\nu_{1/2}$ = 1820 cm^{-1}; and for E_{IVCT} = 5670 cm^{-1}, ϵ = 7700 M^{-1} cm^{-1}, $\nu_{1/2}$ = 1630 cm^{-1}. Plots of the deconvoluted IVCT bands are provided in the Supporting Information. The bandwidths of both intervalence transitions are far smaller than that predicted by the Hush model, a characteristic of strongly coupled systems.[40] Indeed, together with the magnitude of the comproportionation constant and the intensity of these IVCT bands, the mixed-valence properties of $\mathbf{2}^{1-}$ are consistent with a delocalized state, although an exact assignment is ambiguous.[40]

Oxidation of **2** is shown in Figure 5b. Upon oxidation, the band at 17 300 cm^{-1} dropped in intensity, while the intensity of the band at 13 210 cm^{-1} slightly increased. A new low-energy band is observed to grow in at ca. 7600 cm^{-1}. A comparison with the oxidation of $Ru_2(ap)_4(C_2SiMe_3)$ (Figure 4b) shows that this low-energy band is not a common feature, being too low in energy, and so we tentatively assign this band to an IVCT transition. Deconvolution of this band assuming a Gaussian band shape yielded the following IVCT band data: E_{IVCT} = 7700 cm^{-1}, ϵ = 11 000 M^{-1} cm^{-1}, $\nu_{1/2}$ = 1820 cm^{-1}. As for the case of one-electron reduction, the mixed-valence properties of $\mathbf{2}^{1+}$ are consistent with a strongly coupled system.

Discussion

On the basis of the results of X-ray diffraction studies of compounds **2** and **4**, all $Ru_2-C_{2m}-Ru_2$ compounds resemble a dumbbell, and the polyyn-diyl becomes increasingly exposed as the chain elongates. The accessible polyyne backbone provides the opportunity to investigate the reactivity of the Ru_2-modified carbon chain, such as the formation of a π-coordination adduct with $Co_2(CO)_8$ or a cycloaddition insertion reaction with a TCNE molecule.[41]

(39) Mosher, P. J.; Yap, G. P. A.; Crutchley, R. J. *Inorg. Chem.* **2001**, *40*, 1189.

(40) Demadis, K. D.; Hartshorn, C. M.; Meyer, T. J. *Chem. Rev.* **2001**, *101*, 2655.

Previously reported type **I** complexes exhibiting high electron mobility are all based on mononuclear electron-rich complexes (M = Mn, Re, Fe, and Ru) as capping units.[11−14] A combination of the low oxidation state of the metal center and the use of electron-rich donor ligand such as phosphines and Cp^{-1} dictates that these compounds are robust toward oxidation but not reduction. In fact, all of them exhibit strong electronic delocalization in the cationic mixed-valence states. Having a more electron-deficient Ru_2(II,III) moiety as the capping unit, compounds **1**−**5** display extensive electron delocalization in their monoanions. The electrochemically resolved coupling over the C_{12} chain in **5** is remarkable, especially considering the redox-robustness of both the mono- and the dianions indicated by the reversible nature of corresponding couples. Electronic coupling over a C_{12} chain was previously observed with CpRe(NO)P caps, although the corresponding couples appeared irreversible.[12] The Ru_2-capped compounds also display electronic delocalization as the monocation with C_2 and C_4 chains.

The distance dependence of coupling between Ru_2 termini mediated by polyyn-diyl bridges is dramatically illustrated by the CVs of compounds **1**, **2**, **4**, and **5** shown in Figure 2 and the variation in comproportionation constants in Table 2. For both the oxidized mixed-valence complexes (**1**, **2**, **4**, and **5**)$^{1+}$ and the reduced mixed-valence complexes (**1**, **2**, **4**, and **5**)$^{1-}$, mixed-valence properties ranged from that of delocalized to that of valence-trapped states. The distance-dependent electronic coupling in mixed-valence systems has been the subject of a recent review[34] and has application to long-range electron transfer in biological systems. It is most often described by an exponential dependence on distance

$$H_{ad} = H_o \exp(-\gamma R)$$

where H_{ad} and H_o are the donor and acceptor wave function resonance exchange at distance R and van der Waals contact, respectively, γ is a decay factor that is a measure of the medium's ability to mediate electronic coupling, and R is the separation between donor and acceptor from van der Waals contact. For the reduced mixed-valence systems (**1**, **2**, **4**, and **5**)$^{1-}$, a rough estimate of $\gamma = 0.064$ Å^{-1} was derived from a ln(H_{ad}) versus R_{Ru-Ru} plot (Figure 6).[42] This result can be compared to that found for pentaammineruthenium(II,III) donor−acceptor systems bridged by polyenes for which the experimental decay slope γ was found to be 0.070 Å^{-1}.[43] The comparable values of γ between the metal-capped polyenes and polyynes indicate that they have similar capacities in mediating electron transfer. We noted that previous studies of nonlinear optical properties[44] and molecular conductivities[45] concluded that polyenes are superior to polyynes.

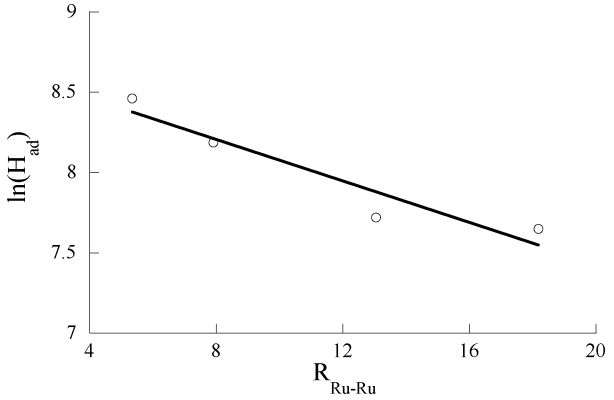

Figure 6. Distance-dependence plot of ln(H_{ad}, in cm^{-1}) versus R_{Ru-Ru} (in Å).

For the complexes in Table 2, an anion mixed-valence complex has a larger K_C value as compared to the cationic mixed-valence complex. A plausible rationale for the origin of this difference is provided below, recognizing that there are other factors besides electronic that contribute to the magnitude of K_C.[43]

In these systems, each diruthenium unit has a ground-state configuration $\sigma^2\pi^4\delta^2(\pi^*)^2(\delta^*)^1$ which is abbreviated as $(\pi^*)^2(\delta^*)^1$.[46] Upon reduction, the resultant Ru_2(II,II) amidinate complexes have a $(\pi^*)^4$ ground-state configuration,[35,47] while the oxidized species, $Ru_2(ap)_4Cl^+$, is best described by a $(\pi^*)^2$ ground-state configuration based on both crystallographic and magnetic evidence.[46] The ramification of this is that, in the cationic or anionic mixed-valence states of **1**, **2**, **4**, and **5**, both donor and acceptor wave functions are of π-symmetry and can mix with the π-symmetry superexchange pathway offered by the polyyn-diyl bridge. Crystallographic evidence (see Results) has shown a contribution of the cumulene resonance form (Scheme 4) to the structure of the polyyne bridge. As this formally involves charge transfer from the dimers to the bridging ligand, superexchange in these mixed-valence systems is best described by the electron-transfer mechanism via the bridging ligand's π-LUMO. The degree of interdimer coupling is then related to the coupling element of each diruthenium with the polyyn-diyl bridge, which is greater in the anion as compared to the cation mixed-valence complexes. Metal−ligand coupling elements can be determined from the spectral data derived from charge-transfer bands.[38] Unfortunately, the appropriate transitions (Ru_2 to polyyn-diyl MLCT) apparently overlap with the LMCT transitions of the $Ru_2(ap)_4$ moiety (see Results) and are not easily deconvoluted.

Conclusions

We have presented the synthesis, structural characterization, voltammetric, spectroscopic, and spectroelectrochemical studies of a new family of carbon-rich organometallic compounds. Both the CV and the spectroelectrochemical results indicate that the polyyne bridges are as efficient as polyenes in mediating electron transfer between two metal termini. Clearly, first principle computations (density functional or ab initio) are necessary to

(41) Bruce, M. I.; Skelton, B. W.; White, A. H.; Zaitseva, N. N. *J. Organomet. Chem.* **2002**, *650*, 141.
(42) For valence-trapped mixed-valence complexes, it is possible to calculate H_{ad} from the free energy of resonance exchange ΔG_r by using the relationship $\Delta G_r = H_{ad}^2/E_{IVCT}$ (see: Evans, C. E. B.; Naklicki, M. L.; Rezvani, A. R.; White, C. A.; Kondratiev, V. V.; Crutchley, R. J. *J. Am. Chem. Soc.* **1998**, *120*, 13096). To obtain a rough estimate of γ, we assumed $2\Delta G_r$ = the free energy of comproportionation and used E_{IVCT} = 8430 cm^{-1} from **2**$^-$. Ru−Ru distances determined from X-ray studies are 7.91 and 13.05 Å for **2** and **4**, respectively, based on which the distances in **1** and **5** were estimated as 5.34 and 18.19 Å, respectively. A plot of ln H_{ad} versus R yields slope $-\gamma$.
(43) (a) Ribou, A. C.; Launay, J. P.; Takahashi, K.; Nihira, T.; Tarutani, S.; Spangler, C. W. *Inorg. Chem.* **1994**, *33*, 1325. (b) Barrière, F.; Camire, N.; Geiger, W. E.; Mueller-Westerhoff, U. T.; Sanders, R. *J. Am. Chem. Soc.* **2002**, *124*, 7262.
(44) Kanis, D. R.; Ratner, M. A.; Marks, T. J. *Chem. Rev.* **1994**, *94*, 195.
(45) Schull, T. L.; Kushmerick, J. G.; Patterson, C. H.; George, C.; Moore, M. H.; Pollack, S. K.; Shashidhar, R. *J. Am. Chem. Soc.* **2003**, *125*, 3202.
(46) Cotton, F. A.; Yokochi, A. *Inorg. Chem.* **1997**, *36*, 567.
(47) Cotton, F. A.; Matusz, M. *J. Am. Chem. Soc.* **1988**, *110*, 5761.

provide the in-depth understanding of both the ground-state electronic structures and the spectroscopic characteristics of these carbon-rich systems. The distance dependence of the spin−spin interaction between two $Ru_2(ap)_4$ units is also of interest and will be explored soon.

Experimental Section

Trimethylsilylacetylene, 1,4-bistrimethylsilyl-1,3-butadiyne, and *n*-BuLi were purchased from Aldrich, CuCl, TMEDA (tetramethylethylenediamine), and Bu_4NF (in THF) were purchased from ACROS, and silica gel was purchased from Merck. $Ru_2(ap)_4Cl$,[21] $Ru_2(ap)_4(C_{2m}Y)$ (m = 1−3, Y = H and $SiMe_3$),[21,48] and 1,6-bistrimethylsilyl-1,3,5-hexatriyne[49] were prepared as previously described. Unless specified, all syntheses were performed using standard Schlenk techniques under an argon atmosphere. THF was distilled over Na/benzophenone under an N_2 atmosphere prior to use. Infrared spectra were recorded on a Perkin-Elmer 2000 FT-IR spectrometer using KBr disks. Vis−NIR spectra in THF were obtained with a Perkin-Elmer Lambda-900 UV−vis−NIR spectrophotometer. Magnetic susceptibility was measured at 294 K with a Johnson Matthey Mark-I magnetic susceptibility balance. Elemental analyses were performed by both the Atlantic Microlab, Norcross, GA, and Galbraith Laboratories, Knoxville, TN. Cyclic voltammograms were recorded in 0.2 M *n*-Bu_4NPF_6 solution (THF, N_2-degassed) on a CHI620A voltammetric analyzer with a glassy carbon working electrode (diameter = 2 mm), a Pt-wire auxiliary electrode, and a Ag/AgCl reference electrode. The concentration of diruthenium species is always 1.0 mM except for **1**, where a 0.47 mM (saturated) solution was used. The ferrocenium/ferrocene couple was observed at 0.573 V (vs Ag/AgCl) at the experimental conditions.

Preparation of $[Ru_2(ap)_4]_2(\mu\text{-}C_2)$ (1). To a 10 mL THF solution containing 0.25 mmol of Me_3SiCCH was added 0.60 mL of BuLi (1.6 M in hexanes) dropwise at room temperature under argon. The mixture was stirred for 8 h to yield a nearly clear solution and was subsequently transferred to a THF (40 mL) solution of $Ru_2(ap)_4Cl$ (0.186 g, 0.20 mmol). While being stirred at room temperature, the solution changed gradually from deep green to brown, and then to reddish-brown overnight. To the ice-chilled reaction solution was added 20 mL of saturated NaCl(aq) solution. The separated organic layer was washed with saturated NaCl(aq) solution until the washings become neutral and was dried over Na_2SO_4. Solvent removal from the organic phase resulted in a purple precipitate, which was collected by filtration and washed with copious amount of CH_2Cl_2. The residue was dried in a vacuum overnight to afford 0.074 g of red-purple microcrystalline materials (42% based on Ru). Data for **1**. Anal. Calcd for $C_{90}H_{72}N_{16}Ru_4$: C, 60.66; H, 4.07; N, 12.58. Found: C, 60.64; H, 4.05; N, 12.35. MS-FAB (*m*/*e*, based on Ru^{101}): 1784 [M^+]. Vis−NIR in THF (λ, nm (ϵ, M^{-1} cm^{-1})): 470 (sh), 559 (36 900), 743 (20 100), 889 (15 600). μ_{eff} (294 K): 5.37 μ_B (μ_{eff}/Ru_2: 3.80 μ_B).

Synthesis of $[Ru_2(ap)_4]_2(\mu\text{-}C_4)$ (2), Method A. To a THF (10 mL) solution of $Me_3SiC_4SiMe_3$ (0.048 g, 0.25 mmol) was added 0.4 mL of 1.6 M BuLi at room temperature under argon. The resultant mixture was stirred for 4 h, and then one-half of the mixture was transferred to a THF (40 mL) solution of $Ru_2(ap)_4Cl$ (0.184 g, 0.20 mmol). The solution changed from deep green to purple-blue in minutes, and the mixture was stirred overnight. The chilled solution was washed with saturated NaCl(aq) solution until the aqueous phase became neutral. Solvent removal from the organic phase led to a purple precipitate, which was filtered and washed with copious amount of CH_2Cl_2 until the rinse became colorless. The purple solid was dried in a vacuum overnight. Yield: 0.096 g (53% based on Ru).

Method B. A 50 mL flask was charged with 0.044 g (0.05 mmol) of $Ru_2(ap)_4(C_2H)$, 0.20 g of $Cu(OAc)_2$, and 15 mL of dry pyridine. The mixture was stirred at room temperature under argon until the complete consumption of $Ru_2(ap)_4(C_2H)$ (5 h). After addition of 20 mL of hexanes and brief stirring, the mixture was filtered. Solvent removal from the filtrate resulted in a purple solid, which was washed with CH_2Cl_2 and water and then dried overnight in vacuo. Yield: 0.015 g (34%).

Data for **2**. Anal. Calcd for $C_{92}H_{72}N_{16}Ru_4$: C, 61.19; H, 4.02; N, 12.41. Found: C, 61.24; H, 4.06; N, 12.37. MS-FAB (*m*/*e*, based on Ru^{101}): 1808 [M^+]. Vis−NIR in THF (λ, nm (ϵ, M^{-1} cm^{-1})): 460 (sh), 579 (37 600), 758 (18 930), 900 (sh). μ_{eff} (294 K): 5.94 μ_B (μ_{eff}/Ru_2: 4.20 μ_B).

Synthesis of $[Ru_2(ap)_4]_2(\mu\text{-}C_6)$ (3). $Me_3SiC_6SiMe_3$ (0.14 g, 0.64 mmol) dissolved in 20 mL of THF was treated with 1.0 mL of 1.6 M BuLi at −20 °C for 2 h. The light brown solution was added to a 90 mL THF solution of $Ru_2(ap)_4Cl$ (1.0 g, 1.1 mmol), and the solution changed from green to reddish-brown upon the completion of the transfer. The reaction slurry was stirred for 8 h at room temperature before being filtered. The solid residue was washed with copious amounts of CH_2Cl_2 and MeOH until the rinse was colorless, and then it was dried in vacuo to yield 0.48 g (47% based on Ru) of dark red solid. Compound **3** is insoluble in all common organic solvents.

Data for **3**. Anal. Calcd for $C_{95}H_{76}N_{16}Cl_2Ru_4$ (**3**·CH_2Cl_2·H_2O): C, 59.04; H, 3.94; N, 11.60. Found: C, 59.00; H, 4.02; N, 11.48. μ_{eff} (294 K): 5.28 μ_B (μ_{eff}/Ru_2: 3.73 μ_B).

Synthesis of $[Ru_2(ap)_4]_2(\mu\text{-}C_8)$ (4). To a THF solution (40 mL) of $Ru_2(ap)_4(C_4H)$ (0.185 g, 0.20 mmol) were added TMEDA (0.050 g, 0.41 mmol) and CuCl (0.010 g, 0.12 mmol). Dry O_2 was bubbled through the solution for 1 h. After solvent removal, the residue was washed carefully with MeOH and extracted with THF. After solvent removal from the extract, the residue was recrystallized from hexanes/CH_2Cl_2 to yield **4** as a red microcrystalline solid. Yield: 0.098 g (53% based on Ru).

Data for **4**. Anal. Calcd for $C_{97}H_{78}N_{16}Cl_2Ru_4$ (**4**·CH_2Cl_2·$2H_2O$): C, 59.00; H, 3.95; N, 11.35. Found: C, 58.88; H, 4.06; N, 11.08. MS-FAB (*m*/*e*, based on Ru^{101}): 1852 [M^+]. Vis−NIR in THF (λ, nm (ϵ, M^{-1} cm^{-1})): 476 (22 720), 581 (14 300), 769 (15 480), 925 (sh). ν(C≡C) (cm^{-1}, KBr disk): 2106 (w), 1940 (w). μ_{eff} (294 K): 5.05 μ_B (μ_{eff}/Ru_2: 3.57 μ_B).

Synthesis of $[Ru_2(ap)_4]_2(\mu\text{-}C_{12})$ (5). A three-necked flask was charged with $Ru_2(ap)_4(C_6H)$ (0.52 mmol, prepared from in situ disilylation of 0.54 g of $Ru_2(ap)_4(C_6TMS)$ with 0.10 mL of TBAF), 0.12 g of TMEDA, 0.03 g of CuCl, and 100 mL of THF. Dry O_2 was bubbled through the solution for 2 h to yield a dark brownish solution. After solvent removal, the residue was washed with methanol and acetone to yield a brownish solid, which was further purified using silica column with the linear gradient of THF/hexanes/Et_3N (v/v/v: 20/80/5 to 50/50/5). Final recrystallization from hexanes/CH_2Cl_2 yielded the analytically pure **5** (0.31 g, 63% based on Ru).

Data for **5**. Anal. Calcd for $C_{102}H_{76}N_{16}Cl_4Ru_4$ (**5**·$2CH_2Cl_2$): C, 59.13; H, 3.67; N, 10.82. Found: C, 59.51; H, 3.72; N, 11.09. MS-FAB (*m*/*e*, based on Ru^{101}): 1903 [MH^+]. Vis−NIR in THF (λ, nm (ϵ, M^{-1} cm^{-1})): 476 (41 450), 777 (16 730), 950 (sh). ν(C≡C) (cm^{-1}, KBr disk): 2133 (w), 2055 (m), 1937 (m). μ_{eff} (294 K): 6.14 μ_B (μ_{eff}/Ru_2: 4.34 μ_B).

Spectroelectrochemistry of 2. An OTTLE cell was used to perform the spectroelectrochemistry.[50] The cell had interior dimensions of roughly 1 × 2 cm with a path length of 0.2 mm and was fitted with a Ag/AgCl reference electrode and ITO (indium−tin oxide) coated glass for the working and counter electrodes. All of the spectroelectrochemical transformations showed good reversibility (greater than 95% recovery of the original complex spectrum).

X-ray Data Collection, Processing, and Structure Analysis and Refinement. Single crystals were grown via either a slow evaporation of a THF solution (**2**) or vapor diffusion of methanol into

(48) Ni, Y. M.S. Thesis, University of Miami, 2001.
(49) Rubin, Y.; Lin, S. S.; Knobler, C. B.; Anthony, J.; Boldi, A. M.; Diederich, F. *J. Am. Chem. Soc.* **1991**, *113*, 6943.
(50) (a) Krejcik, M.; Danek, M.; Hartl, F. *J. Electroanal. Chem.* **1991**, *317*, 179. (b) Evans, C. E. B. Ph.D. Thesis, Carleton University, 1997.

THF solution (**4**). The X-ray intensity data were measured at 300 K on a Bruker SMART1000 CCD-based X-ray diffractometer system using Mo Kα ($\lambda = 0.71073$ Å). A thin plate of dimension $0.32 \times 0.17 \times 0.005$ mm^3 cemented onto a quartz fiber with epoxy glue and a block of dimension $0.25 \times 0.21 \times 0.06$ mm^3 wedged in a capillary filled with mother liquor were used for the data collection of **2** and **4**, respectively. Data were measured using ω scans of 0.3° per frame such that a hemisphere (1271 frames) was collected. No decay was indicated for any of three data sets by the recollection of the first 50 frames at the end of data collections. The frames were integrated with the Bruker SAINT software package[51] using a narrow-frame integration algorithm, which also corrects for the Lorentz and polarization effects. Absorption corrections were applied using SADABS supplied by George Sheldrick.

The structures were solved and refined using the Bruker SHELXTL (version 5.1) software package[52] in the space group $P\bar{1}$ for both crystals **2** and **4**. Positions of all non-hydrogen atoms of diruthenium moieties were revealed by the direct method. The asymmetric unit of **2** contains halves of two independent molecules, which are related to the other halves by crystallographic inversion centers. Four water molecules were also located in the asymmetric unit of **2**. The asymmetric unit of **4** contains one THF and one methanol molecule in addition to one-half of the independent molecule, and the latter is related to the other half by a crystallographic inversion center. With all non-hydrogen atoms being anisotropic and all hydrogen atoms in the calculated position and riding mode, the structure was refined to convergence by the least-squares method on F^2, SHELXL-93, incorporated in SHELXTL.PC v. 5.03. Relevant information on the data collection and the figures of merit of final refinement are listed in Table 3.

Table 3. Crystallographic Parameters for Compounds **2**·8H_2O and **4**·THF·MeOH

	2·8H_2O	**4**·THF·MeOH
formula	$C_{92}H_{88}N_{16}O_8Ru_4$	$C_{106}H_{96}N_{16}O_4Ru_4$
fw	1950.1	2062.27
space group	$P\bar{1}$	$P\bar{1}$
a (Å)	10.084(2)	10.1620(1)
b (Å)	20.023(3)	13.0260(1)
c (Å)	22.504(4)	19.802(2)
α (deg)	95.518(3)	71.838
β (deg)	95.250(3)	77.106
γ (deg)	93.827(4)	81.34
volume (Å^3)	4491(1)	2418.6(5)
Z	2	1
d_{calc} (g cm^{-3})	1.442	1.416
μ (mm^{-1})	0.724	0.673
radiation	Mo Kα	Mo Kα
T (K)	300(2)	300(2)
R1, wR2	0.075, 0.185	0.068, 0.153

Acknowledgment. Research at the University of Miami was supported in part by the Petroleum Research Fund/ACS (36595-AC3), the National Science Foundation (CHE 0242623), and the University of Miami (diffractometer fund). Research performed at the Carleton University was supported by the Natural Sciences and Engineering Research Council of Canada (NSERC). G.-L.X. and M.C.D. thank the University of Miami for a Maytag graduate fellowship and NSERC for a postgraduate scholarship, respectively.

Supporting Information Available: Plots of deconvoluted IVCT bands in both $\mathbf{2}^{+1}$ and $\mathbf{2}^{-1}$, DPV plots for compounds **1**−**5**, spectroelectrochemical data for $Ru_2(ap)_4(C_4SiMe_3)$ (PDF), and X-ray crystallographic files in CIF format for the structure determination of compounds **2** and **4**. This material is available free of charge via the Internet at http://pubs.acs.org.

JA035434J

(51) *SAINT V 6.035 Software for the CCD Detector System*; Bruker-AXS Inc., 1999.

(52) (a) *SHELXTL 5.03 (WINDOW−NT Version), Program library for Structure Solution and Molecular Graphics*; Bruker-AXS Inc., 1998. (b) Sheldrick, G. M. *SHELXL-93, Program for the Refinement of Crystal Structures*; University of Göttigen, Germany, 1993. (c) Sheldrick, G. M. *SHELXS-90, Program for the Solution of Crystal Structures*; University of Göttigen, Germany, 1990.